Nano Energy 55 (2019) 49–58

Contents lists available at ScienceDirect

Nano Energy

journal homepage: www.elsevier.com/locate/nanoen

Full paper

RuO_2 nanocluster as a 4-in-1 electrocatalyst for hydrogen and oxygen electrochemistry

Han-Saem Park[a,1], Juchan Yang[a,1], Min Kyung Cho[b], Yeongdae Lee[a], Seonghun Cho[c], Sung-Dae Yim[c], Byeong-Su Kim[d], Jong Hyun Jang[b,*], Hyun-Kon Song[a,*]

[a] School of Energy and Chemical Engineering, Ulsan National Institute of Science and Technology, UNIST-gil 50, Ulsan 44919, Republic of Korea
[b] Fuel Cell Research Center, Korea Institute of Science and Technology (KIST), Hwarangno 14-gil 5, Seongbuk-gu, Seoul 02792, Republic of Korea
[c] Fuel Cell Laboratory, Korea Institute of Energy Research (KIER), 152 Gajeong-ro, Daejeon 34129, Republic of Korea
[d] Department of Chemistry, Yonsei University, 50, Yonsei-ro, Seodaemun-gu, Seoul 03721, Republic of Korea

ARTICLE INFO

Keywords:
Multi-functional electrocatalysts
Water splitting
Carbon coated metal oxides
All-pH electrolysis
Regenerative fuel cells

ABSTRACT

Partially hydrous RuO_2 nanocluster embedded in a carbon matrix (*x*-RuO_2@C with *x* = hydration degree = *0.27* or *0.27*@C) is presented as a bifunctional catalyst for hydrogen evolution reaction (HER) and oxygen evolution reaction (OER) for water splitting. Symmetric water electrolyzers based on *0.27*-RuO_2@C for both electrodes showed smaller potential gaps between HER and OER at pH 0, pH 14 and even pH 7 than conventional asymmetric electrolyzers based on two different catalysts (Pt/C || Ir/C) that have been known as the best catalysts for HER and OER respectively. Moreover, *0.27*-RuO_2@C showed another bifunctional electroactivity for fuel cell electrochemistry involving hydrogen oxidation reaction (HOR) and oxygen reduction reaction (ORR) that are the backward reactions of HER and OER respectively. Pt-level HOR electroactivity was obtained from *0.27*-RuO_2@C, while its ORR activity was inferior to that of Pt with 200 mV higher overpotential required. The tetra-functionality of *0.27*-RuO_2@C showed the possibility of realizing single-catalyst regenerative fuel cells.

1. Introduction

Hydrogen economy is one of the possible and potential alternatives to the present hydrocarbon economy even if the concept has been criticized in terms of its low conversion efficiencies and infeasible competitive edge over other energy sources. Hydrogen production and its conversion to electricity are the starting and ending points of hydrogen economy, respectively. In the interim between them, hydrogen storage and its transportation are another important sectors in hydrogen economy [1]. Water electrolysis is one of the main production methods, which is more environmentally friendly than the steam reformation of hydrocarbons is. However, water electrolysis has the disadvantages of high cost and low efficiencies [2–5]. Electrocatalysts have been developed to improve water electrolysis efficiencies while renewable energy sources were combined with electrolyzers for cost reduction [6,7]. On the other hand, various types of fuel cells have been considered as candidates for hydrogen/electricity conversion [8]. As a more advanced hydrogen-based device, regenerative fuel cells function as water electrolyzers to produce hydrogen in its regenerative or reverse mode and as fuel cells to generate electricity in its fuel cell mode [9]. The core element of electrolyzers and fuel cells is electrocatalysts that accelerate kinetics of hydrogen evolution reaction (HER) and oxygen evolution reaction (OER) for water electrolysis; and hydrogen oxidation reaction (HOR) and oxygen reduction reaction (ORR) for fuel cells. HER and OER are the backward reactions of HOR and ORR, respectively. In this work, we introduce a single catalyst for all the four reactions, demonstrating successful operation of symmetric water electrolyzers.

Electrochemical water splitting occurs through two reactions: HER at $E^\circ = 0\ V_{RHE}$ (E° = standard reduction potential, V_{RHE} = V versus RHE) and OER at 1.23 V_{RHE}.

	Acid	Base	
HER:	$2H^+ + 2e^- \rightarrow H_2$	$2H_2O + 2e^- \rightarrow H_2 + 2OH^-$	(1)
OER:	$2H_2O \rightarrow O_2 + 4H^+ + 4e^-$	$2OH^- \rightarrow O_2 + 2H_2O + 4e^-$	(2)

Two issues are most challenging in the field of electrocatalysts for water electrolysis: (1) bifunctional catalysts covering both HER and OER; and (2) HER or OER catalysts working over a wide pH range [10–12].

First, high-performance monofunctional catalysts such as Pt for HER

* Corresponding authors.
E-mail addresses: jhjang@kist.re.kr (J.H. Jang), philiphobi@unist.ac.kr, philiphobi@hotmail.com (H.-K. Song).
[1] Authors contributed equally to this work.

https://doi.org/10.1016/j.nanoen.2018.10.017
Received 27 April 2018; Received in revised form 21 September 2018; Accepted 8 October 2018
Available online 23 October 2018

and Ir, Ru and their oxides for OER have been developed. However, there are limited reports on HER/OER-bifunctional catalysts covering both the reactions for water electrolysis. Transition metal oxides, sulfides, and phosphates were developed as bifunctional catalysts for HER and OER [13–17]. Moreover, ORR in addition to HER and OER was covered by single-catalyst systems such as doped or defective graphenes and their composites with metal oxides [18–21]. However, their electroactivities were far below those of the well-known monofunctional catalysts. Ru-based catalysts are considered a candidate for HER/OER bifunctional catalysts, which is supported by two recent publications [22,23]. Bifunctional catalysts possibly simplify water electrolysis systems because a single catalyst covers both of the electrodes [24]. In conventional asymmetric electrolyzers, the HER catalysts are different from the OER catalysts. The OER electrode compartment is exposed to oxidative environments while the HER compartment experiences reductive potential. The long-term oxidative and reductive loads on electrodes possibly deteriorate or corrode the parts of electrolyzers. On the other hand, symmetric electrolyzers based on single bifunctional catalysts can be operated by switching the electrodes periodically. Thus, more durable operation of water electrolysis is expected [25].

Second, HER catalysts developed until now favors acid media while OER catalysts work efficiently in alkaline media [2,12,26]. Therefore, it is difficult to pair the best HER catalysts with the best OER catalysts at a fixed pH for water electrolysis. Alkaline electrolytes have been widely used for mass hydrogen production so that developing high-HER-electroactivity catalysts at high pH is of great importance [13,23,27]. Alternatively, catalysts guaranteeing high OER electroactivities and stability in acid media open extended opportunities for acid electrolyzer [24,28,29]. On the other hand, electrolyte around pH 7 is the poorest media for water electrolysis because both H_2 and O_2 are generated from water molecules instead of H^+ and OH^-. Water electrolysis based on neutral media, if possible, has the benefits of safety, low cost and corrosion-free conditions [12,30,31].

In our previous work [32], we demonstrated ORR/OER bifunctionality of RuO_2-based catalysts in *alkaline* media. RuO_2 has been known as one of the best OER catalysts; however, its ORR activity was unexpected before. The key factor controlling both ORR and OER activities was hydration degree of RuO_2. Hydrous RuO_2 (often described by $RuO_2{\cdot}nH_2O$ with n = hydration degree) is a composite of anhydrous rutile-like RuO_2 nanocrystals dispersed by boundaries of structural water associated with Ru-O [33]. Partial hydration improved OER kinetics on RuO_2: the current at 1.6 V_{RHE} of a partially hydrated RuO_2 was more than 10 times as high as that of totally anhydrous RuO_2. Moreover, the partial hydration significantly reduced overpotentials of ORR by ~200 mV at $-3\,mA\,cm_{disk}^{-2}$. Herein, we extended the OER/ORR electroactivity of RuO_2 to HER. Recently, a Ru-based electrocatalyst was reported to show platinum-level HER activities while its cost is only ~4% of that of Pt [22]. The partially hydrated RuO_2 of this work showed both OER and HER electroactivities for water electrolysis over a wide range of pH including pH = 0, 7, and 14. The catalyst reported in this work is the first bifunctional water-splitting catalyst that works *at all pH* and shows high electroactivities for both HER and OER. Xue et al. reported the HER/OER bifunctional electroactivities of Co/CoP at universal pH; however, its OER activities were seriously inferior to the reported values of OER activities of monofunctional catalysts [34]. A *symmetric* electrolyzer based on the single catalyst was realized, which is characterized by a small overpotential. It was superior to the *asymmetric* electrolyzer based on Pt and Ir considered as the best pair for water splitting.

As an additional extension, we demonstrated that the HER/OER catalyst covered both HOR and ORR. Unified regenerative fuel cells (URFCs) is a form of regenerative fuel cells (RFCs), where hydrogen as well as electricity is generated in a single device (Fig. S1) [9,35,36]. Hydrogen is produced by splitting water by renewable electricity such as solar and wind powers (electrolysis mode), which is used as a fuel to generate electricity in the same device (fuel cell mode). HER and OER proceed on negative and positive electrodes respectively in the electrolysis mode. On the other hand, HOR and ORR occurs on the corresponding electrodes during the fuel cell mode. URFCs is more cost-effective than discrete regenerative fuel cells (DRFCs) consisting of separate devices of an electrolyzer and a fuel cell [36]. A single tetrafunctional catalyst, instead of a cocktail of multiple mono-functional catalysts or two bifunctional catalysts (one for HER and HOR while the other for OER and ORR), is the ideal catalyst to realize the challenging URFCs in a more performance-guaranteeing and cost-effective way [9]. A 4-in-1 electrocatalyst has not been reported so far, even if tri-functional catalysts for HER, OER and ORR are available [18–21].

2. Materials and methods

2.1. *x*-RuO_2@C as catalyst

Partially hydrated RuO_2 (*x*-RuO_2@C) was synthesized as described in our previous work [32]. Briefly, aqueous suspension of hydrous RuO_2 nanoparticles templated by PEO_{5000}-*b*-PAA_{6700} (numbers in subscript = molecular weights of each block; Polymer Source) were prepared from an aqueous mixture of the block copolymer, NaOH, $RuCl_3{\cdot}xH_2O$ (Sigma-Aldrich) and hydrazine (N_2H_4; Sigma-Aldrich). The dried suspension was annealed at 400 °C for 2 h to form *x*-RuO_2@C. Totally anhydrous RuO_2 (*ah*-RuO_2; 30–50 nm primary particles from Sigma-Aldrich) and totally hydrous RuO_2 (*h*-RuO_2; 100–200 nm primary particles from Alfa Aesar) were used as received for comparison (Fig. S1). Pt/C (20 wt% Pt on carbon black, Alfa Aesar) and Ir/C (20 wt% Ir on carbon black, Premetek) were also used for comparison.

2.2. Relative hydration degree *x*

The existence of OH^- and Ru^{3+} indicates the hydrous phase of ruthenium oxide while O^{2-} and Ru^{4+} identifies the anhydrous phase. The amount of each identity was quantified by fitting X-ray photoelectron spectra (XPS). 3 component spectra were used for deconvoluting O1s XPS spectra: lattice oxygen (O^{2-}) at 530.4 eV; hydroxyl group (OH^-) at 531.2 eV; and surface-bound water (H_2O) at 532.5 eV. 6 component spectra were used for deconvoluting Ru3d and C1s XPS spectra: Ru (IV) indicating RuO_2 at 281.0 and 285.5 eV; Ru(III) of hydrous Ru(III)-OH at 281.7 and 286.4 eV; C 1 s at 284.6 and 288.5 eV. The peak area ratio of OH^- to O^{2-} (OH^-/O^{2-}) or Ru^{3+} to Ru^{4+} (Ru^{3+}/Ru^{4+}) was used as a measure of the hydration degree. The OH^-/O^{2-} of *ah*-RuO_2 and *h*-RuO_2 were 0.80 and 2.40, respectively. The Ru^{3+}/Ru^{4+} of *ah*-RuO_2 and *h*-RuO_2 were 1.34 and 2.61, respectively. *ah*-RuO_2 and *h*-RuO_2 were assumed to be 0% and 100% hydrated (x = 0 and 1), respectively. Calibration curves were obtained by linear regression of the two points. The *relative* hydration degrees (x) were read from the calibration curves. Two values of x estimated from the OH^-/O^{2-} and Ru^{3+}/Ru^{4+} calibration curves were averaged.

2.3. Characterization

Catalysts were characterized by transmission and scanning electron microscopes (JEOL JEM-2100F for TEM and Hitach S-4800 for SEM) and X-ray diffraction (XRD; Rigaku D/MAX 2500V/PC with Cu–Kα radiation (λ = 1.5418 Å) at 35 kV and 20 mA).

2.4. Catalyst inks

Homogeneous catalyst inks were prepared by dispersing 8 mg catalyst composite (*x*-RuO_2@C) and 2 mg Ketjen Black 600 in a mixture of 450 μl of ethanol and 50 μl of 5 wt% Nafion solution (Sigma-Aldrich, 274704) by using sonication for 30 min 6 μl of the catalyst ink was dropped onto a polished glassy carbon (GC, 0.1256 cm^2) disk of rotating ring disk electrodes (RRDE with Pt ring/GC disk; ALS, A-011162) and then fully dried at ambient temperature. The resultant catalyst loading

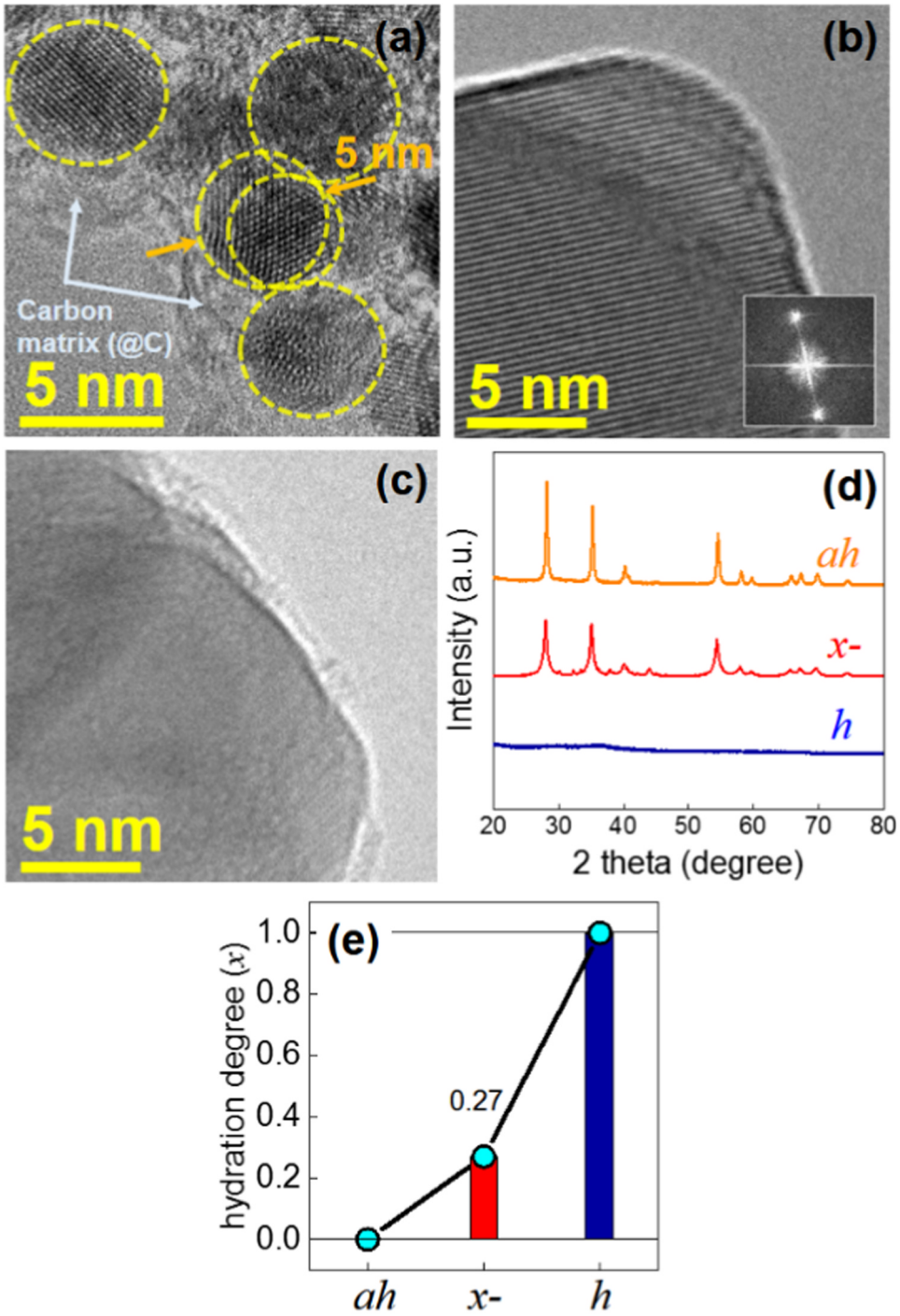

Fig. 1. Partially hydrous ruthenium oxide embedded in carbon (*x*-RuO_2@C). (a–c) TEM images: a = *x*-RuO_2 @C; b = anhydrous RuO_2 (*ah*-RuO_2); c = hydrous RuO_2 (*h*-RuO_2). (d) XRD patterns of *x*-, *ah*- and *h*-RuO_2. (e) Relative hydration degree (*x*) of RuO_2-based catalysts. Refer to Experimental section for calculating *x*.

density was 96 μg_{cat} cm_{disk}^{-2}. In addition to the synthesized *x*-RuO_2 @C, anhydrous (Sigma-Aldrich, 238058) and hydrous (Alfa Aesar, 43403) ruthenium oxides (*ah*- and *h*-RuO_2) were used as control catalysts in the same composition. Also, 60 wt% Pt on carbon black (Alpha Aesar, 35849, HiSPEC 3000) and 20 wt% Ir on Vulcan XC72 (Premetek, P40A200) were used as control catalyst composites for HER and OER, respectively. Loading density of Pt/C and Ir/C was 96 μg_{cat} cm_{disk}^{-2} and 24 μg_{cat} cm_{disk}^{-2}, respectively.

2.5. Electrochemistry

The polarization curves were obtained in 3-electrode configuration including RRDEs by a potentiostat (Bio-Logic VMP3). Catalyst-loaded RRDE as working electrode was immersed in a glass cell containing 0.5 M H_2SO_4 (pH 0), 1 M phosphate buffer solution (pH 7), 0.1 M KOH (pH 13) and 1 M KOH (pH 14). Ag/AgCl (RE-1B, ALS; pH 0 and 7)) or Hg/HgO (XR400, Radiometer Analytical; pH 13 and 14) was used as the

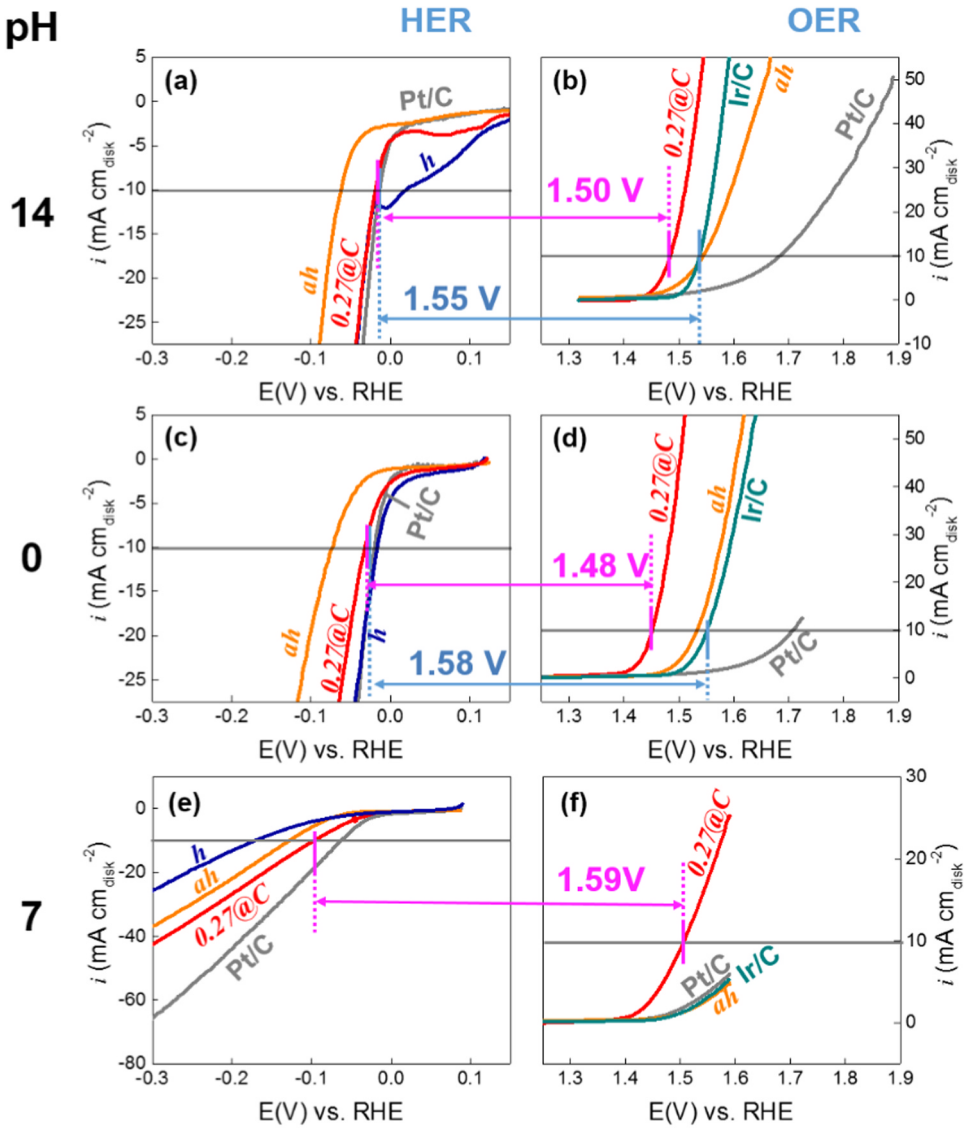

Fig. 2. HER and OER polarization. The plots in the left and right columns are for HER and OER, respectively. Three different electrolytes were used: 1 M KOH at pH 14 (**a** and **b**); 0.5 M H_2SO_4 at pH 0 (**c** and **d**); and 1 M phosphate buffer solution (PBS) at pH 7 (**e** and **f**). Rotating disk electrodes of glassy carbon in 0.1256 cm^2 were used at 1600 rpm. Currents were normalized by the geometric area of disk electrode (cm_{disk}^{-2}). 20 wt% carbon black was used for ruthenium-oxide-based catalysts. ***h*** = *h*-RuO_2; ***ah*** = *ah*-RuO_2; ***0.27*@C** = *0.27*-RuO_2@C.

reference electrode. Pt wire or graphite rod was used as the counter electrode. No electroactivity improvements by the use of Pt counter electrode due to its dissolution and following deposition on working electrodes [37] were confirmed by repeating the same experiments with the two different counter electrodes (Refer to Fig. S7 for confirming no difference of HER polarization of *0.27*-RuO_2@C during 2000 times repeated potential sweeps between Pt wire and graphite rod counter electrodes). The HER and OER polarization voltammograms at 10 mV s^{-1} were obtained in N_2-purged electrolytes at 1600 rpm. The HOR and ORR polarization curves were recorded in the H_2- and O_2-saturated electrolytes at 1600 rpm with a scan rate of 10 mV s^{-1}. Unless otherwise noted, all polarization curves were iR (f = 85%) corrected by using the EC-Lab software. Potentials were reported as the values versus reversible hydrogen electrode (RHE) in V_{RHE} (V versus RHE). Exchange currents (i_o), as a kinetics descriptor, were estimated by using Tafel equation. All electrochemical data were obtained at room temperature.

2.6. Water splitting

Lab-made water electrolyzer was constructed. 100 µl catalyst ink was loaded on 1 cm^2 carbon papers (Toray TGP-H-0930) for acidic electrolytes or porous nickel foams (MTI EQ-bcnf-16m) for alkaline electrolytes. Catalyst loading density was fixed at 0.8 mg_{cat} cm^{-2}. The catalyst-loaded electrodes were dried at 80 °C for > 1 h. Two catalyst-loaded electrodes were immersed in an electrolyte-containing acrylic container equipped with 20 ml graduated gas collectors. 1 M KOH (aq) or 0.5 M H_2SO_4 (aq) was used as electrolyte. Water was electrolyzed potentiostatically by using 1.5 V AA batteries or galvanostatically by using a galvanostat (Bio-Logic, VMP3).

2.7. Alkaline anion exchange membrane water electrolyzer (AEMWE)

AEMWEs were made by sandwiching an alkaline anion exchange membrane between two identical electrodes. Graphite blocks designed for allowing serpentine flows of electrolytes backed up the electrodes, which were contacted to aluminium end plates. *0.27*-RuO_2@C was loaded at 1.0 mg cm^{-2} on carbon papers (TGP-H-120, Toray) in the presence of 20 wt% ionomer (fumion® FAA-3 solution, Fumatech). The electrodes and an anion exchange membrane (fumasep® FAA-3-PK-75, Fumatech) were stored in 1.0 M KOH solution for 24 h to exchange

bromide anions of ionomers to hydroxide ions, followed by washing with distilled water to remove excess KOH solution. The AEMWEs were operated at room temperature with 0.5 M KOH solution as the feed solutions for both anode and cathode. Linear sweep voltammograms were obtained between 1.4 V_{cell} to 2.0 V_{cell} at 20 mV s^{-1} before potentiostatic operations at 1.6 V_{cell}. Electrochemical impedance spectra (EIS) were obtained at 1.6 V_{cell} in 30 kHz to 30 mHz with a sinusoidal amplitude at 10 mV.

3. Results and discussion

3.1. X-RuO_2@C as catalyst

Partially hydrated RuO_2 was synthesized as a form of nanoclusters comprising 5-nm RuO_2 nanoparticles embedded in a continuous carbon matrix phase (*x*-RuO_2@C in Fig. 1a) [32,38]. Electroactivities of *x*-RuO_2@C were compared with those of totally anhydrous RuO_2 and totally hydrous RuO_2 in this work (*ah*-RuO_2 in Fig. 1b and *h*-RuO_2 in Fig. 1c, respectively). The hydrated phase (*h*-RuO_2) was amorphous while the anhydrous or partially hydrous RuO_2 showed crystalline phases (Fig. 1d). The relative hydration degree (*x*) of *x*-RuO_2@C prepared at 400 °C was estimated at 0.27 when the hydration degrees of *ah*-RuO_2 and *h*-RuO_2 were taken as 0 and 1, respectively (Fig. 1e). Annealing temperatures determined hydration degrees and then electroactivities. The most optimized sample showing the well balanced multi-functionality in this work was *0.27*-RuO_2@C that was annealed at 400 °C. The samples synthesized from five different batches at the same annealing temperature showed hydration degrees between 0.25 and 0.29: average = 0.266 with standard deviation = 0.0167. Their electroactivities were estimated very close to each other. Hydration numbers decreased with increasing temperature (Fig. S3). *0.5*-RuO_2@C and *0.14*-RuO_2@C, more and less highly hydrous catalysts than *0.27*-RuO_2@C, were obtained at 350 °C and 450 °C, respectively. Higher hydration degree supported more improved HER and OER activities (Fig. S4). However, the stability of OER activities of too hydrous samples (*0.5*-RuO_2@C) was not guaranteed (0.5@C of Fig. S4b).

3.2. HER

The HER electroactivity of *0.27*-RuO_2@C (or shortly *0.27*@C) in 1 M KOH at pH 14 was comparable to or even better than that of Pt/C that is known as the best HER catalyst (Fig. 2a and Fig. S5a). The onset potentials of *0.27*-RuO_2@C and Pt/C were identical while a higher HER current was obtained by *0.27*-RuO_2@C at high overpotentials. The hydrated phase was considered beneficial for HER electroactivity because partially or totally hydrous RuO_2 (*0.27*-RuO_2@C and *h*-RuO_2) was superior to *ah*-RuO_2 in terms of HER onset potentials. The kinetics of *0.27*-RuO_2@C was superior to that of *h*-RuO_2 especially at high overpotentials probably due to the carbon matrix (@C) providing a conductive environment to *0.27*-RuO_2. The HER activity of *0.27*-RuO_2@C became more inferior to that of Pt/C as the electrolyte was changed from alkaline to acidic (0.5 M sulfuric acid at pH 0) to neutral (1 M phosphate buffer solution at pH 7) (Fig. 2c and e and Fig. S5c; Fig. S6c for Tafel plots). It should be emphasized that the HER activities of *0.27*-RuO_2@C were superior to those of any other *multi-functional* catalysts ever reported over the entire pH range covering basic, acidic and neutral media (Fig. 3a and Table S1). For example, an overpotential less than 100 mV was required by *0.27*-RuO_2@C for HER to extract $-10\ mA\ cm_{disk}^{-2}$ in a neutral medium that is the poorest medium for water splitting. Much higher overpotentials were required at the same current density by previously reported catalysts: 140 mV by Co/CoP nanoparticles [34]; 337 mV by CoO/$CoSe_2$ nanobelts [39]; 480 mV by N or S co-doped graphitic sheets [20]. Even more improved electroactivities of *0.27*-RuO_2 @C were observed up to 1500 potential sweeps between +0.2 V_{RHE} and −0.2 V_{RHE} in 1 M KOH (aq) (Fig. S7). The current density at −0.2 V_{RHE} at the 1500th cycle was 1.5 times that at the 1st cycle. Insignificant current changes in the polarization curves were observed after the 1500th cycle. The HER durability is contrasted with that of Pt/C showing electroactivity decay during long-term cycle tests [22].

The effects of hydration on HER electroactivities are understood from a mechanistic standpoint. There are two mechanisms for HER: Vomer-Heyrovsky and Volmer-Tafel pathways [40,41].

$$\text{-Ru-O} + H_2O + e^- \rightarrow \text{-Ru-OH} + OH^- \text{ (Volmer)} \quad (3)$$

$$\text{-Ru-OH} + H_2O + e^- \rightarrow \text{-Ru-O} + H_2 + OH^- \text{ (Heyrovsky)} \quad (4)$$

$$\text{-Ru-OH} + \text{HO-Ru-} \rightarrow 2\ \text{-Ru-O} + H_2 \text{ (Tafel)} \quad (5)$$

In the Volmer step as the first step of both pathways, a proton is adsorbed on a surface dehydrogenated oxygen species (-Ru-O) by the help of an electron. The Volmer step is a more sluggish process when compared with Heyrovsky and Tafel steps as indicated by their Tafel slopes. Larger Tafel slopes originate from slower kinetics, requiring larger potential difference for obtaining a fixed current difference. The Tafel slope (*b*) of the Volmer step is known to be 120 mV dec^{-1}, which is much larger than 40 mV dec^{-1} for the Heyrovsky step and 30 mV dec^{-1} for the Tafel step [40,41]. The surface hydroxyl species (-Ru-OH) resulting from the Volmer step lead to hydrogen evolution via Heyrovsky or Tafel step. The HER on the totally anhydrous RuO_2 (*ah*-RuO_2) showed the largest Tafel slopes (> 60 mV dec^{-1} in Fig. S6a and e) at pH 14 and 0 among RuO_2 samples. That is to say, the HER pathway of *ah*-RuO_2 is more Volmer-determining than that of other RuO_2, leading to the most sluggish process. On the other hand, Tafel slopes of hydrous RuO_2 (*0.27*-RuO_2@C and *h*-RuO_2) were closer to 40 mV dec^{-1} than that of *ah*-RuO_2 (Fig. S6a and e). That is to say, hydration moved the rate determining step (RDS) from more Volmer-determining pathway to less Volmer-determining and more Heyrovsky-determining one. The abundantly pre-existent –Ru-OH in hydrous RuO_2 possibly allow the Volmer step of hydrogen adsorption *not* to limit the overall kinetics. Also, -Ru-O generated after Heyrovsky step in the hydrous RuO_2 appears to catch protons from electrolyte in a fast manner as expected from the smaller value of Tafel slope. In the same vein, a previous work suggested that multivalent ruthenium oxyspecies on surface possibly acted as a metastable cyclic redox mediator system in HER [42]. Ru^{3+} in -O-Ru(III)$(OH)_2$ was reduced to Ru^{2+} in -O-Ru(II)(OH)(OH_2) and then Ru^+ in -O-Ru(I)$(OH_2)_2$. In the following step, Ru^+ was returned to Ru^{3+} while H_2 was evolved. The facile kinetics of the closed reduction-oxidation cycles improves the overall HER kinetics.

3.3. OER

RuO_2 has been reported as one of the best OER electrocatalysts in acidic as well as in basic electrolytes [43]. In the Pourbaix diagram of Ru, dissolved phases as RuO_4^-, RuO_4^{2-}, and $HRuO_5^-$ are thermodynamically favored at high pH and over 1.1 V_{RHE} [44]. However, it was reported that ruthenium oxide generated after the first anodic and cathodic potential sweep of Ru metal showed a stable OER current during the following repeated scans [45]. *h*-RuO_2 (not shown) was the most superior in terms of onset potential, which was followed by *0.27*-RuO_2@C and then *ah*-RuO_2 for all pH conditions (Fig. 2b, d and f; Fig. S5b and d). However, the totally hydrated form was unstable in alkaline media so that no OER current was obtained after the initial anodic scan. *0.27*-RuO_2@C was superior to any other catalysts including Pt/C and even Ir/C (known as one of the best OER catalysts) for OER over the entire range of pH. The Tafel slopes (*b*) of *0.*27-RuO_2@C were more similar to those of Ir/C rather than those of *ah*-RuO_2 and Pt/C (Fig. S6b, d and f). OER in neutral media have begun to be reported very recently even if the activities in neutral media are much lower than those in acidic and basic media. The low ionic conductivities of neutral media are partially responsible for the large overpotentials of the electrochemical reactions. In spite of the demerits, neutral media have

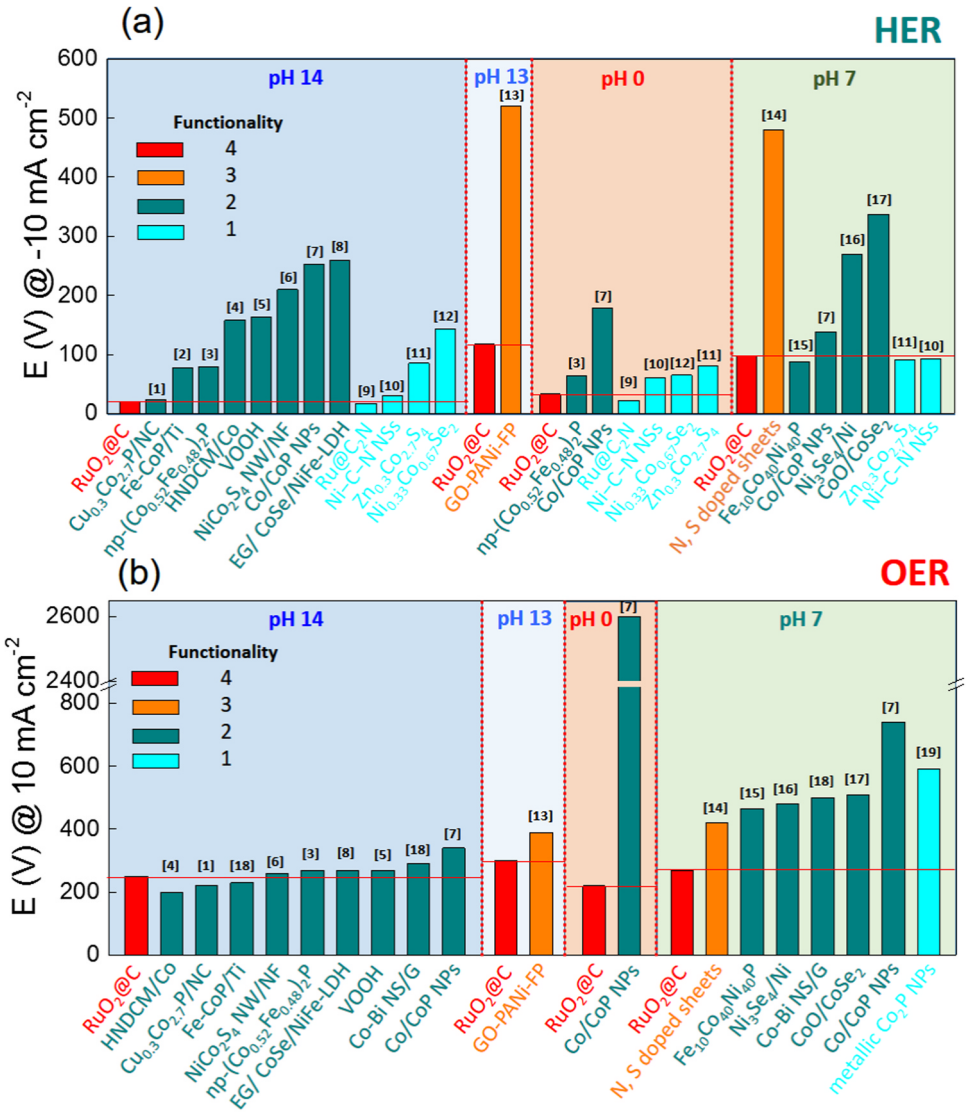

Fig. 3. Overpotentials of HER and OER at ± 10 mA cm^{-2}. Overpotentials of this work were compared with those of reported multifunctional catalysts in HER (**a**) and OER (**b**). Four different electrolytes were used: 1 M KOH at pH 14; 0.1 M KOH at pH 13; 0.5 M H_2SO_4 at pH 0; and 1 M phosphate buffer solution (PBS) at pH 7. The bibliographic information of the reference numbers is found in Table S1 and S2 in Supporting Information.

advantages such as eco-friendliness and cost effectiveness over non-neutral media [46]. *0.27*-RuO_2@C showed incomparably lower overpotentials than the recently reported catalysts in neutral media (Fig. S8) [20,46].

The OER on metal oxide is known to follow a four-step mechanism where the second and third steps are the rate determining step (RDS; Eqs. (7) and (8)) [47]:

$$\text{-Ru-OH} + \text{OH}^- \rightarrow \text{-Ru-O} + \text{H}_2\text{O} + \text{e}^- \quad (6)$$

$$\text{-Ru-O} + \text{OH}^- \rightarrow \text{-Ru-OOH} + \text{e}^- \text{ (RDS)} \quad (7)$$

$$\text{-Ru-OOH} + \text{OH}^- \rightarrow \text{-Ru-OO} + \text{H}_2\text{O} + \text{e}^- \text{ (RDS)} \quad (8)$$

$$\text{-Ru-OO} + \text{OH}^- \rightarrow \text{-Ru-OH} + \text{O}_2 + \text{e}^- \quad (9)$$

The abundantly pre-existent hydroxyl species (-Ru-OH) in hydrous RuO_2 possibly accelerates the deprotonation step (Eq. (6)) to generate the oxyspecies (-Ru-O). The highly concentrated -Ru-O improves the kinetics of the following RDS (Eq. (7)). Proton conduction allowed in hydrous RuO_2 could play a considerable role in improving OER kinetics. The OER electrocatalytic superiority of *0.27*-RuO_2@C was considered to originate partly from its appropriate hydration degree. The hydrous form was highly OER-active but unstable while the anhydrous form was stable but inferior OER-kinetically. Electrically conductive environment provided by the carbon matrix (@C) surrounding the RuO_2 would be helpful in improving the kinetics. It was difficult to find catalysts showing higher OER electroactivities than that of *0.27*-RuO_2 @C in acidic and neutral media in literature (Fig. 3b and Table S2). A single work [34] (Co/CoP) reported multi-functional catalysts in all pH, showing OER overpotentials of 340 mV at 10 mA cm^{-2} in alkaline media, 570 mV at 1.3 mA cm^{-2} in acid and 570 mV at 2.64 mA cm^{-2} in neutral media. Much smaller overpotentials were obtained by *0.27*-RuO_2 @C: 250 mV at 10 mA cm^{-2} in the same alkaline media, 170 mV at 1.3 mA cm^{-2} in the same acidic media and ~220 mV at 2.77 mA cm^{-2} in the same neutral media.

Both intensive properties (e.g., electroactivities per catalyst area or mass) and extensive properties (e.g., catalyst loading amounts) determine device-level performances (e.g., electroactivities per geometric area of electrodes or devices, used in Fig. 2). Higher loading amounts of catalysts do not necessarily guarantee an increase in catalytic currents due to the problems related to electron conduction and mass transfer. High-loading metal catalysts on carbon supports (e.g., 80 wt% Pt/C) do not necessarily result in high activities due to the increase in metal

particle size beyond its optimized value (3–5 nm for Pt) and particle agglomeration during operation. The *0.27*-RuO_2@C has oxide particles separated by carbon wraps. Therefore, it is relatively easy to increase its loading without suffering from the activity loss. Also, the cost issues should be considered for heavy loading of catalysts. The price of RuO_2 is one hundredth to one thousandth of the price of Pt metal.

We used catalytic currents normalized by electrode area in HER/OER polarization curves (Fig. 2). For an intensive-property comparison between *0.27*-RuO_2@C and the best novel metal catalysts (Pt/C for HER or Ir/C for OER), the catalytic currents were normalized by surface area or mass of catalysts to eliminate the effects of catalyst loading amounts (Fig. S9). It should be notified that catalyst loading amounts were different between RuO_2 and Pt or Ir as the controls. *0.27*-RuO_2@C occupied 80 wt% of total weight of catalyst layer including catalyst and carbon black. Pt and Ir was loaded at 60 wt% and 20 wt% on carbon support without additional carbon black, respectively. The total amounts of the catalyst layers in weight were fixed for all catalysts. Catalyst areas were calculated from catalyst densities under the assumption of spherical shapes of catalysts: catalyst area = 3 × mass / density / mean radius [48]. When the polarization curves were compared in terms of currents normalized by the catalyst surface area or mass, the HER and OER activities of *0.27*-RuO_2@C are still high and competitive with the activities of the best novel metal catalysts.

3.4. Water splitting

Water electrolysis performances were expected from the HER and OER polarizations (Fig. 2). The overpotential gap between HER and OER required to extract 10 or 100 mA cm_{disk}^{-2} ($\Delta E_{\pm 10}$ and $\Delta E_{\pm 100}$) was estimated as a measure of the performances (Fig. 4**a** and Fig. S10). The smallest overpotential gap, $\Delta E_{\pm 10}$, was obtained in alkaline media by *0.27*-RuO_2@C, which is superior to that of a pair of Pt for HER and Ir for OER: $\Delta E_{\pm 10}$ ($\Delta E_{\pm 100}$) = 1.50 (1.69) V for *0.27*-RuO_2@C||*0.27*-RuO_2@C versus 1.56 (1.79) V for Pt/C||Ir/C (Fig. 2a and b). The electrolysis performance of *0.27*-RuO_2@C is surprising when considering that Pt/C||Ir/C is the best combination of catalysts that have ever been reported. In addition, the value of $\Delta E_{\pm 10}$ of *0.27*-RuO_2@C is very close to the theoretical potential gap at 1.23 V for water splitting. When compared with the reported symmetric electrolyzers based on a single catalyst, the *0.27*-RuO_2@C showed top-level performances (Fig. 4b; Table S3) [4,16,49,50]. The polarization curve of our cell (solid line in pink) was well matched with the difference between the OER and ORR half-cell polarization data (circles in pink).

Water was electrolyzed into oxygen and hydrogen in electrolyzers with alkaline media at 3 V by two 1.5 V commercially available AA batteries in series (inset of Fig. 4c; Water was split even by one 1.5 V AA battery, as shown in Fig. S11a and Movie S1). Hydrogen and oxygen gases were generated vigorously (Fig. S11a and b and Movie S1) at the expected stoichiometric ratio (H_2:O_2 = 2:1) for all the examined pairs of catalysts. The electrolysis time to obtain 20 ml H_2 was shortest in the *0.27*-RuO_2 @C||*0.27*-RuO_2 @C electrolyzer (Fig. 4c). Water splitting was very stable in the presence of *0.27*-RuO_2@C for > 110 h without any obvious voltage changes at 10 and 20 mA cm^{-2} in 1 M KOH (Fig. S12), confirming that *0.27*-RuO_2@C electrolyzed water into hydrogen and oxygen without any side reactions for long-term operations.

Supplementary material related to this article can be found online at doi:10.1016/j.nanoen.2018.10.017.

Following the successful operation of the symmetric electrolyzers in beaker-type configurations, anion exchange membrane water electrolyzers (AEMWE) were constructed for confirming more practical operations. *0.27*-RuO_2 @C was used for both electrodes in 0.5 M KOH at room temperature (Fig. S13a). The AEMWE based on *0.27*-RuO_2 @C ||*0.27*-RuO_2 @C was also successfully operated in a way similar to the beaker-type cell. The onset potential of water splitting was estimated at ~1.4 V on a potential sweep (Fig. S13b); this value coincided with that of the beaker-type symmetric electrolyzers (Fig. 4b). The polarization curve of AEMWE approximated that of the beaker-type electrolyzer. Electroactivities of *0.27*-RuO_2 @C were significantly improved during the initial 4 h period in the potentiostatic operation at 1.6 V, showing an increase in current from 16 mA cm^{-2} to 40 mA cm^{-2} (Fig. S13c). The current was then saturated after 4 h. The initial increase in electrolysis currents was ascribed to the decrease in charge transfer resistances estimated by diameters of semi-circles in impedance spectra (Fig. S13d). Br^- of the anion exchange membranes would be further exchanged with OH^- in the initial period. Also, catalyst layers containing catalyst particles and ionomers are possibly evolved to have a

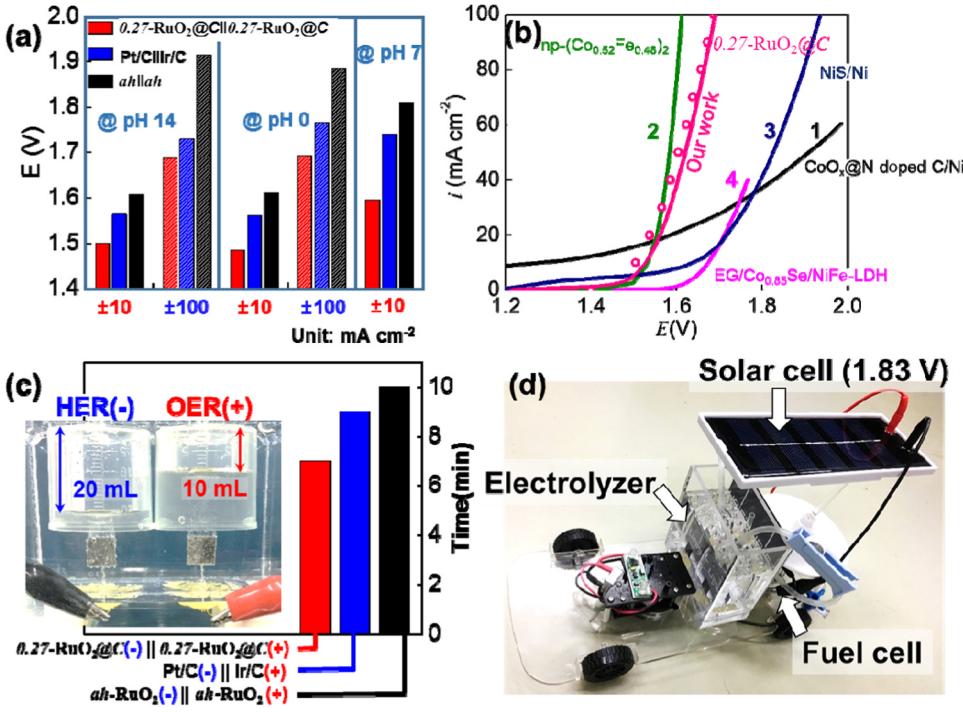

Fig. 4. Symmetric water electrolyzer. Catalysts were loaded on 1 cm^2 of nickel electrodes. (**a**) Overpotential gap between HER and OER ($\Delta E_{OER-HER}$) at 10 or 100 mA cm^{-2}. (**b**) Polarization curves of this work in comparison with those of previously reported symmetric electrolyzers. 1 = ref 2,15. = ref 3. = ref 4,39. = ref. 38. (**c**) Electrolysis time required to obtain 20 ml H_2. Inset photo = the symmetric electrolyzer. (**d**) A miniaturized fuel-cell car driven by hydrogen generated by the *0.27*-RuO_2 @C||*0.27*-RuO_2 @C electrolyzer powered by a solar cell at 1.83 V. Electrolyte = 1 M KOH for **b** and **c** and 0.5 M H_2SO_4 for **d**.

morphological structure integrated with efficient mass and electron transfer pathways by experiencing ionomer swelling and gas evolution. The AEMWE was superior to the beaker-type cells even if more dilute electrolyte was used (0.5 M KOH for AEMWE versus 1.0 M KOH for beaker-type). Higher currents were obtained in the AEMWE when compared with the beaker-type water electrolyzer (Fig. S13 for the AEMWE versus Fig. S12 for the beaker cell): 40 mA cm^{-2} for the AEMWE versus 10 mA cm^{-2} for the beaker type at ~1.6 V.

In addition to alkaline electrolysis, acid electrolysis was investigated at 0.5 M H_2SO_4 at pH 0. The HER overpotentials in acid were similar to or slightly larger than those in alkaline electrolyte (Fig. 2c and Fig. S6c). Even if *h*-RuO_2 was superior to *0.27*-RuO_2@C in HER, it was very unstable in OER. The best OER polarization was obtained by *0.27*-RuO_2@C while the HER of *0.27*-RuO_2@C was inferior to that of Pt/C (Fig. 2d and Fig. S5d). The resultant overpotential gaps were similar to those obtained in the alkaline media: $\Delta E_{\pm 10}$ ($\Delta E_{\pm 100}$) = 1.48 (1.69) V for *0.27*-RuO_2@C||*0.27*-RuO_2@C versus 1.56 (1.77) V for Pt/C||Ir/C (Fig. 4a**)**. Real operation of the symmetric electrolyzer based on *0.27*-RuO_2@C as catalysts for both the electrodes in acid was confirmed by demonstrating the successful driving of a miniaturized fuel-cell car using the hydrogen generated by our electrolyzer powered by a silicon solar cell at 1.83 V (Fig. 4d and Movie S2).

Supplementary material related to this article can be found online at doi:10.1016/j.nanoen.2018.10.017.

Recently, OER electrocatalysts working in neutral media have been reported (Fig. 3b; Table S2) [31,46,51,52]. Unlike in acid and alkaline media, large overpotentials were required to extract meaningful currents of electrolysis. In phosphate buffer solution (PBS) at pH 7 (Fig. 2e and f), *0.27*-RuO_2@C was uncompetitive with Pt/C in HER. However, its OER superiority was more prominent over other catalysts in neutral media than in other non-neutral media. The OER currents at 10 mA cm_{disk}^{-2} were read only for *0.27*-RuO_2@C when the potential was anodically scanned up to 1.6 V_{RHE}. The $\Delta E_{\pm 10}$ of *0.27*-RuO_2 @C||*0.27*-RuO_2@C was estimated at 1.59 V, which is similar to those of acid and alkaline media for the same catalysts and much smaller than that of Pt/C||Ir/C at 1.74 V. The OER superiority of *0.27*-RuO_2 @C in neutral media was confirmed by comparing with other works (Fig. 3b, Fig. S8 and Table S2).

One of the merits of the use of HER/OER bifunctional catalysts in water electrolyzers, as we suggested in introduction, is the *alternating* operation by switching electrodes for HER and OER. More durable operation of water electrolysis is expected by the *alternating* operation compared with the conventional *biased* operation. Unwanted events such as carbon corrosion during OER could be suppressed in the alternating operation by avoiding long-term exposure to oxidative (or reductive) environments. An alternating operation and two biased operations were compared (Fig. S14). For the alternating operation, − 10 mA cm^{-2} for 10 min followed by + 10 mA cm^{-2} for another 10 min was applied repeatedly to *0.27*-RuO_2@C loaded on disk electrode. The same currents were applied for OER and HER-biased operations during the entire time period. The differences of electrochemical signals were not clearly identified before magnifying the potential plateau regions (the inset of Fig. S14). Overpotentials were developed less over time when the alternating operation was adopted instead of the biased operation. The overpotential gains especially in OER by the alternating operation are thought to be due to hydration of the surface oxide of RuO_2 during the precedent HER operations. Hydration was beneficial in both HER and OER but too much hydration resulted in an OER instability as shown above (Fig. 3 and S4). Overpotential difference between 20 min and 2 h in the alternating operation was 12 mV, very close to that of the OER-biased operation (15 mV). However, the cell experiencing the HER-biased operation for 3 h before the OER-biased operation showed a more serious increase in overpotential (38 mV). It indicates that the temporal partitioning of an electric load effectively reduced or delayed the instability.

3.5. Tetra-functionality: ORR & HOR in addition to HER & OER

ORR and HOR are the basic principle reactions for hydrogen fuel cells. In hydrogen economy, the fuel cells generate electricity by using the hydrogen generated by water electrolyzers. The ORR and HOR are the reverse reactions of OER and HER, respectively. In addition to its

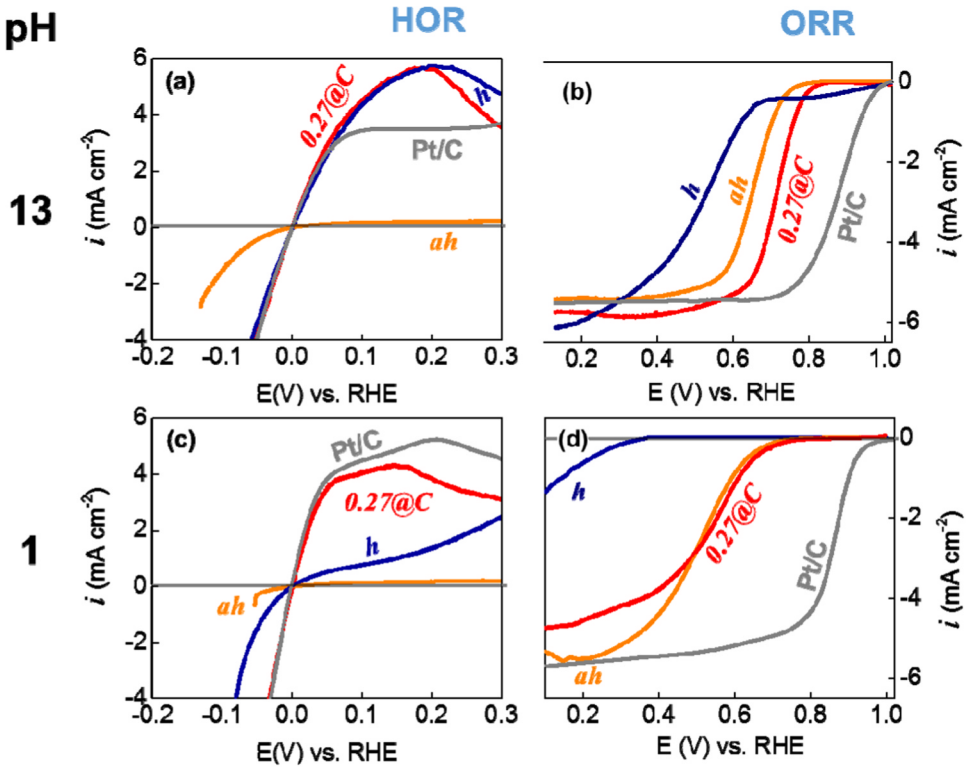

Fig. 5. HOR and ORR polarization. (**a** to **d**) Polarization curves. The plots in the left and right columns are for HOR and ORR, respectively. Two different electrolytes were used: 0.1 M KOH at pH 13 (**a** and **b**) and 0.1 M $HClO_4$ at pH 1 (**c** and **d**). Rotating disk electrodes of glassy carbon in 0.1256 cm^2 were used at 1600 rpm. 20 wt% carbon black was used for ruthenium-oxide-based catalysts. ***h*** = *h*-RuO_2; ***ah*** = *ah*-RuO_2; ***0.27@C*** = *0.27*-RuO_2 @C.

OER and HER activities, the ruthenium oxide catalysts were investigated in terms of ORR and HOR. Our final goal is to develop a single catalyst for hydrogen economy. Reversible operation between fuel cells and electrolyzers would be possible with the single tetrafunctional catalyst. In this work, the feasibility of *0.27*-RuO_2@C as ORR and HOR catalysts was examined.

The ORR electroactivity of RuO_2 has been rarely reported while its OER activity has been widely investigated. Poor electroactivities characterized by low ORR currents and high overpotentials have been reported with RuO_2 [53–55]. As an example, the potential at a half of the limiting current ($E_{2/L}$ at $i_L/2$) was + 0.56 V_{RHE} at − 1.2 mA cm_{disk}^{-2} (cf. +0.9 V_{RHE} at −3 mA cm_{disk}^{-2} for Pt/C) [54]. The high overpotential indicates very sluggish ORR kinetics on RuO_2. More seriously, electron transfer number (n) was estimated at ~2 (4 is preferred for n; discussed below). In our previous work [32], interestingly, much higher ORR electroactivities in alkaline media were obtained even from the *ah*-RuO_2 as the control. When compared with *h*-RuO_2 and *ah*-RuO_2, our *0.27*-RuO_2 @C showed the merits of both forms of RuO_2 (Fig. 5**b**). In the conductive environments achieved by 20 wt% carbon black, *ah*-RuO_2 was favored in terms of the onset potential in ORR polarization. On the other hand, *h*-RuO_2 was favored in terms of the number of electron transfer (n) especially at low overpotentials. The thermal treatment at 400 °C (*0.08*-RuO_2 in Fig. 5) improved the high overpotential of *h*-RuO_2, shifting the onset potential to that of *ah*-RuO_2.

Following the investigation on ORR activity, the HOR electroactivity of *0.27*-RuO_2@C was confirmed. *h*-RuO_2 showed good HOR electroactivity comparable to that of Pt/C while *ah*-RuO_2 was not HOR-active in both acid and alkaline media (Fig. 5**a** and **c**). The Pt-level HOR activities of *0.27*-RuO_2@C were higher than those of Ru/Ir alloy catalysts reported in a previous work: maximum current at pH 13 = 6 mA cm_{disk}^{-2} for our *0.27*-RuO_2@C versus 3 mA cm_{disk}^{-2} for Ru/Ir alloy in the literature [56]. For obtaining intensive properties by eliminating the effects of catalyst loading amounts, the currents were normalized by catalyst surface area (in cm_{cat}^2) and catalyst mass (in mg_{cat}) in addition to geometric electrode area (in cm_{disk}^2). In the intensive-property comparison (Fig. S9 and S15), the HOR activities of *0.27*-RuO_2@C were still high, approaching the activities of the Pt/C.

4. Conclusion

In this work, a single electrocatalyst was presented, which was able to electrocatalyze four different electrochemical reactions related to hydrogen and oxygen. Partially hydrous ruthenium oxide (*0.27*-RuO_2@C) as the 4-in-1 catalyst demonstrated incomparable OER activity and Pt-level HER/HOR activities with significantly improved ORR activity superior to that of pristine ruthenium oxide. In addition, it should be emphasized that the catalyst retained its catalytic superiority over the entire range of pH even including neutral media. We demonstrated the usefulness of the multifunctional catalyst by showing the successful operation of symmetric water electrolyzers. Also, we suggest the possibility of URFC operating with 4-in-1 catalysts in this work even if there are many technical hurdles that should be overcome. The operation of the single-catalyst URFC is on-going in our laboratory.

Acknowledgements

This work was supported by National Research Foundation (GPF: 2016H1A2A1909427, Climate change: 2017M1A2A2087813), Korea Carbon Capture & Sequestration R&D Center (2014M1A8A1049296) and Ministry of Education (BK21Plus: 10Z20130011057), Republic of Korea.

Competing financial interests

The authors declare no competing financial interests.

Appendix A. Supporting information

Supplementary data associated with this article can be found in the online version at doi:10.1016/j.nanoen.2018.10.017.

References

[1] M.P. Suh, H.J. Park, T.K. Prasad, D.W. Lim, Chem. Rev. 112 (2012) 782–835.
[2] J. Wang, F. Xu, H. Jin, Y. Chen, Y. Wang, Adv. Mater. 29 (2017) (1605838-1605838).
[3] Z.-F. Huang, J. Song, K. Li, M. Tahir, Y.-T. Wang, L. Pan, L. Wang, X. Zhang, J.-J. Zou, J. Am. Chem. Soc. 138 (2016) 1359–1365.
[4] Y. Tan, H. Wang, P. Liu, Y. Shen, C. Cheng, A. Hirata, T. Fujita, Z. Tang, M. Chen, Energy Environ. Sci. 9 (2016) 2257–2261.
[5] J. Durst, A. Siebel, C. Simon, F. Hasche, J. Herranz, Ha Gasteiger, Energy Environ. Sci. 7 (2014) 2255–2260.
[6] C.C.L. McCrory, S. Jung, I.M. Ferrer, S.M. Chatman, J.C. Peters, T.F. Jaramillo, J. Am. Chem. Soc. 137 (2015) 4347–4357.
[7] J. Jia, L.C. Seitz, J.D. Benck, Y. Huo, Y. Chen, J.W.D. Ng, T. Bilir, J.S. Harris, T.F. Jaramillo, Nat. Commun. 7 (2016) (13237-13237).
[8] B.C. Steele, A. Heinzel, Nature 414 (2001) 345–352.
[9] J.W. Desmond, Ng, Y. Gorlin, T. Hatsukade, T.F. Jaramillo, Adv. Energy Mater. 3 (2013) 1545–1550.
[10] L. Jingshan, I. Jeong-Hyeok, M.T. Mayer, M. Schreier, M.K. Nazeeruddfn, P. Nam-Gyu, S.D. Tilley, F. Hong Jin, M. Gratzel, Science 345 (2014) 1593–1596.
[11] J. Tian, Q. Liu, A.M. Asiri, X. Sun, J. Am. Chem. Soc. 136 (2014) 7587–7590.
[12] D. Liu, Q. Lu, Y. Luo, X. Sun, A.M. Asiri, Nanoscale 7 (2015) 15122–15126.
[13] A. Sivanantham, P. Ganesan, S. Shanmugam, Adv. Funct. Mater. 26 (2016) 4661–4672.
[14] Y. Yang, H. Fei, G. Ruan, J.M. Tour, Adv. Mater. 27 (2015) 3175–3180.
[15] H. Wang, H.-W. Lee, Y. Deng, Z. Lu, P.-C. Hsu, Y. Liu, D. Lin, Y. Cui, Nat. Commun. 6 (2015) (7261-7261).
[16] H. Jin, J. Wang, D. Su, Z. Wei, Z. Pang, Y. Wang, J. Am. Chem. Soc. 137 (2015) 2688–2694.
[17] H. Zhu, L. Gu, D. Yu, Y. Sun, M. Wan, M. Zhang, L. Wang, L. Wang, W. Wu, J. Yao, M. Du, S. Guo, Energy Environ. Sci. 10 (2017) 321–330.
[18] J. Zhang, L. Dai, Angew. Chem. Int. Ed. 55 (2016) 13296–13300.
[19] Y. Jia, L. Zhang, A. Du, G. Gao, J. Chen, X. Yan, C.L. Brown, X. Yao, Adv. Mater. 28 (2016) 9532–9538.
[20] C. Hu, L. Dai, Adv. Mater. 29 (2016) (1604942-1604942).
[21] X. Liu, W. Liu, M. Ko, M. Park, M.G. Kim, P. Oh, S. Chae, S. Park, A. Casimir, G. Wu, J. Cho, Adv. Funct. Mater. 25 (2015) 5799–5808.
[22] J. Mahmood, F. Li, S.-M. Jung, M.S. Okyay, I. Ahmad, S.-J. Kim, N. Park, H.Y. Jeong, J.-B. Baek, Nat. Nanotechnol. (2017) 1–7.
[23] Y. Zheng, Y. Jiao, Y. Zhu, L.H. Li, Y. Han, Y. Chen, M. Jaroniec, S.-Z. Qiao, J. Am. Chem. Soc. 138 (2016) 16174–16181.
[24] J. Wang, W. Cui, Q. Liu, Z. Xing, A.M. Asiri, X. Sun, Adv. Mater. 28 (2016) 215–230.
[25] B.C.M. Martindale, E. Reisner, Adv. Energy Mater. 6 (2016) (1502095-1502095).
[26] X. Zou, X. Huang, A. Goswami, R. Silva, B.R. Sathe, E. Mikmeková, T. Asefa, Angew. Chem. 126 (2014) 4461–4465.
[27] M.E.G. Lyons, R.L. Doyle, M.P. Brandon, Phys. Chem. Chem. Phys. 13 (2011) 21530–21551.
[28] T. Kwon, H. Hwang, Y.J. Sa, J. Park, H. Baik, S.H. Joo, K. Lee, Adv. Funct. Mater. 27 (2017) (1604688-1604688).
[29] T. Reier, M. Oezaslan, P. Strasser, ACS Catal. 2 (2012) 1765–1772.
[30] X. Elias, Q. Liu, C. Gimbert-Suriñach, R. Matheu, P. Mantilla-Perez, A. Martinez-Otero, X. Sala, J. Martorell, A. Llobet, ACS Catal. 6 (2016) 3310–3316.
[31] P. Chen, K. Xu, T. Zhou, Y. Tong, J. Wu, H. Cheng, X. Lu, H. Ding, C. Wu, Y. Xie, Angew. Chem. Int. Ed. 55 (2016) 2488–2492.
[32] H.-S. Park, E. Seo, J. Yang, Y. Lee, B.-S. Kim, H.-K. Song, Sci. Rep. 7 (2017) (7150-7150).
[33] W. Dmowski, T. Egami, K.E. Swider-Lyons, C.T. Love, D.R. Rolison, J. Phys. Chem. B 106 (2002) 12677–12683.
[34] Z.-H. Xue, H. Su, Q.-Y. Yu, B. Zhang, H.-H. Wang, X.-H. Li, J.-S. Chen, Adv. Energy Mater. (2017) (1602355-1602355).
[35] E. Antolini, ACS Catal. 4 (2014) 1426–1440.
[36] B.S. Lee, H.Y. Park, M.K. Cho, J.W. Jung, H.J. Kim, D. Henkensmeier, S.J. Yoo, J.Y. Kim, S. Park, K.Y. Lee, J.H. Jang, Electrochem. Commun. 64 (2016) 14–17.
[37] R. Chen, C. Yang, W. Cai, H.-Y. Wang, J. Miao, L. Zhang, S. Chen, B. Liu, ACS Energy Lett. 2 (2017) 1070–1075.
[38] E. Seo, T. Lee, K.T. Lee, H.-K. Song, B.-S. Kim, J. Mater. Chem. 22 (2012) 11598–11604.
[39] K. Li, J. Zhang, R. Wu, Y. Yu, B. Zhang, Adv. Sci. 3 (2016) 1500426.
[40] X. Gao, H. Zhang, Q. Li, X. Yu, Z. Hong, X. Zhang, C. Liang, Z. Lin, Angew. Chem. Int. Ed. 55 (2016) 6290–6294.
[41] Y. Zhu, W. Zhou, Y. Zhong, Y. Bu, X. Chen, Q. Zhong, M. Liu, Z. Shao, Adv. Energy Mater. 7 (2017) 10–17.
[42] L.D. Burke, N.S. Naser, J. Appl. Electrochem. 35 (2005) 931–938.
[43] Y. Jiao, Y. Zheng, M. Jaroniec, S.Z. Qiao, Chem. Soc. Rev. 44 (2015) 2060–2086.
[44] I. Povar, O. Spinu, J. Electrochem. Sci. Eng. 6 (2016) (145-145).
[45] R. Kötz, J. Electrochem. Soc. 130 (1983) (825-825).
[46] K. Xu, H. Cheng, L. Liu, H. Lv, X. Wu, C. Wu, Y. Xie, Nano Lett. 17 (2017) 578–583.
[47] W.T. Hong, M. Risch, K.A. Stoerzinger, A. Grimaud, J. Suntivich, Y. Shao-Horn, Energy Environ. Sci. 8 (2015) 1404–1427.

[48] H. Wang, Hc.D. Abru?a, J. Am. Chem. Soc. 139 (2017) 6807–6810.
[49] Y. Hou, M.R. Lohe, J. Zhang, S. Liu, X. Zhuang, X. Feng, Energy Environ. Sci. 9 (2016) 478–483.
[50] W. Zhu, X. Yue, W. Zhang, S. Yu, Y. Zhang, J. Wang, J. Wang, Chem. Commun. 1 (2016) 3–6.
[51] Y. Liu, C. Xiao, M. Lyu, Y. Lin, W. Cai, P. Huang, W. Tong, Y. Zou, Y. Xie, Angew. Chem. Int. Ed. 54 (2015) 11231–11235.
[52] K. Jin, J. Park, J. Lee, K.D. Yang, G.K. Pradhan, U. Sim, D. Jeong, H.L. Jang, S. Park, D. Kim, N.-E. Sung, S.H. Kim, S. Han, K.T. Nam, J. Am. Chem. Soc. 136 (2014) 7435–7443.
[53] H. Jiang, Y. Yao, Y. Zhu, Y. Liu, Y. Su, X. Yang, C. Li, ACS Appl. Mater. Interfaces 7 (2015) 21511–21520.
[54] J. Masa, W. Xia, I. Sinev, A. Zhao, Z. Sun, S. Grützke, P. Weide, M. Muhler, W. Schuhmann, Angew. Chem. Int. Ed. 53 (2014) 8508–8512.
[55] J. Sunarso, aM. Glushenkov, aaJ. Torriero, P.C. Howlett, Y. Chen, D.R. MacFarlane, M. Forsyth, J. Electrochem. Soc. 160 (2012) H74–H79.
[56] J. Ohyama, D. Kumada, A. Satsuma, J. Mater. Chem. A 4 (2016) 15980–15985.

Dr. Han-Saem Park received his B.S. degree in mechanical engineering at the Kyungpook University in 2010. And he obtained his Ph.D. degree in Energy Engineering at UNIST (Ulsan National Institute of Science and Technology) in 2018. He currently works as a senior researcher at LG Chem/Research Park. His research focus on multi-functional electrocatalyst for electrochemical energy conversion devices such as regenerative fuel cells and metal air cells.

Dr. Juchan Yang received his B.S. degree in 2009 and M.S. degree in 2011 in Materials Science and Engineering from Inha University. From 2012–2013, he then worked as a researcher in Department of Chemistry at University of Kentucky, USA. He obtained his Ph.D. degree from Energy Engineering at UNIST (Ulsan National Institute of Science and Technology) in 2018 under the supervision of Prof. Hyun-Kon Song. He is currently a postdoctoral fellow in KIMS (Korea Institute of Materials Science). His research focus on the design of oxygen and hydrogen electrocatalyst for high activity and durability.

Min Kyung Cho is a postdoctoral reseracher at Fuel Cell Research Center of Korea Institute of Science and Technology (KIST). She received her Ph. D. degree from Seoul National University in 2017. Her research activities include characterization and optimization of electrode/MEA for electrochemical energy conversion devices such as fuel cell and water electrolyzer.

Yeongdae Lee received his B.S. degrees from the Ulsan National Institute of Science and Technology (UNIST) in Ulsan, Korea, in 2015. He is currently in the process of Ph.D. course in UNIST. His research interests focus on demonstrating the effect of metal-support interaction on the activity and durability of oxygen electrocatalysts.

Dr. Seonghun Cho received his Ph.D. degree from University of Science and Technology (UST) in Daejeon, Korea, in 2018. Currently, he works as a postdoctoral researcher at the University of Yamanashi, Kofu, Japan. His current research interests mainly include design of catalyst layer and understanding of water transport on the catalyst layer in polymer electrolytes fuel cells.

Dr. Sung-Dae Yim is a principal researcher at the Fuel Cell Laboratory in Korea Institute of Energy Research (KIER) since 2003. He received his Ph.D. in Chemical Engineering from Pohang University of Science and Technology (POSTECH) in 2001. His research interests include design of cathode catalyst layers and membrane electrode assembly (MEA) for Polymer Electrolyte Membrane (PEM) fuel cell applications.

Dr. Byeong-Su Kim is Associate Professor of Department of Chemistry at Yonsei University, Korea. He received Ph.D. in Chemistry at the University of Minnesota in 2007. After a postdoctoral researches at MIT, he started his independent career at UNIST since 2009 and moved to Yonsei University in 2018. His research and education program cover a broad span of macromolecular chemistry in the study of novel polymer and hybrid nanomaterials, including the molecular design and synthesis of self-assembled polymers, layer-by-layer assembly for functional thin films, and now expand to complex macromolecular systems such as carbon nanomaterials.

Dr. Jong Hyun Jang is a principal researcher at the Fuel Cell Research Center of Korea Institute of Science and Technology (KIST). He received his Ph. D. degree in Chemical Technology from Seoul National University, Korea, in 2004. He was a postdoctoral researcher at Tokyo University of Agriculture and Technology and Newcastle University. His current research focuses on catalyst/MEA development and electrochemical analysis of various polymer electrolyte membrane (PEM)-based electrochemical devices: PEMFC, water electrolyzer, electrochemical CO_2 conversion, and electrochemical hydrogen pump.

Prof. Hyun-Kon Song is a professor of School of Energy and Chemical Engineering at UNIST, Korea. He received his Ph.D. degree in Chemical Engineering from POSTECH, Korea. He was a postdoctoral researcher at Brown University and Seoul National University, and a senior researcher at LG Chem/Research Park. He is an electrochemist who is interested in charge transfer kinetics in electrocatalysis, molecular interaction between constituents of electrolytes and novel design of electrochemistry-based devices.